Bias dependence and inversion of the tunneling magnetoresistance in ferromagnetic junctions

Fei-fei Li, Zheng-zhong Li, Ming-wen Xiao, Jun Du, Wang Xu, and An Hu
National Laboratory of Solid State Microstructures, Department of Physics, Nanjing University, Nanjing 210093, China
(Received 12 July 2003; revised manuscript received 13 October 2003; published 17 February 2004)

This paper presents a microscopic theory for spin-polarized tunneling in the FM/I/FM junction under a finite applied voltage. A significant decrease of the tunneling magnetoresistance (TMR) with increasing bias is obtained from the theory. We note that the spin-dependent prefactor of the transmission coefficient plays an important role in the tunneling. In particular, the bias-dependent quantum-coherence factor $\kappa_R^2(E_x,V) - k_{R\uparrow}(E_x,V)k_{R\downarrow}(E_x,V)$ rather than the density of states controls the sign change of TMR at finite voltage. The effects of an asymmetric potential profile within the barrier region is calculated in comparison with the tunneling junctions of the composite barrier (Al_2O_3/Ta_2O_5). Numerical results are in qualitative agreement with experiments.

DOI: 10.1103/PhysRevB.69.054410 PACS number(s): 75.70.Cn, 72.10.Fk, 72.10.Di

I. INTRODUCTION

Electron tunneling through an insulating barrier between two normal-metal electrodes with identical number of up-spin and down-spin electrons has been studied experimentally and theoretically since the 1920s.[1] In the 1960s, Harrison[2] discussed the tunneling theory within independent-particle approximation, and verified the applicability of the WKB approximation. Afterwards, Brinkman and co-workers[3] and Simmons[4] confirmed further the availability of the WKB approximation for bias-dependent tunneling in normal-metal junctions. In the 1970s Tedrow and Meservey[5] introduced the concept of spin-polarized tunneling, where the amounts of electrons for each spin are unequal. Their earlier study on the conservation of spin during tunneling laid the foundation for the new research field of spin-dependent tunneling. Jullière[6] made the first FM-I-FM trilayer junction which showed a larger conductance for parallel magnetization alignment of the two ferromagnetic electrodes than that of antiparallel alignment. Furthermore, Jullière also presented a qualitative model to explain the change of conductance between different alignments, and defined the tunneling magnetoresistance (TMR),

$$\mathrm{TMR}=\frac{G_P-G_{AP}}{G_P}=\frac{2PP'}{1+PP'}, \tag{1}$$

where P and P' are the spin polarization of the left and right ferromagnetic electrodes expressed as

$$P=\frac{N_\uparrow-N_\downarrow}{N_\uparrow+N_\downarrow}, \quad P'=\frac{N'_\uparrow-N'_\downarrow}{N'_\uparrow+N'_\downarrow}, \tag{2}$$

where $N_\uparrow$ and $N_\downarrow$ are the densities of states (DOS's) at Fermi level of the left electrode, and $N'_\uparrow$ and $N'_\downarrow$ are the ones for the right electrode. In Jullière model, the left and right electrodes are treated separately, and the tunneling matrix elements are independent of momentum and energy. As a result, the tunneling current of each spin channel is proportional to the product of the DOS's of the two electrodes for given spin channel. However, the independence of TMR on the geometry and the electronic structure of the barrier assumed by Eq. (2) is unrealistic, which has already been pointed out by MacLaren and co-workers.[7] By a full quantum-mechanical treatment, Slonczewski[8] developed a better expression for the TMR,

$$\mathrm{TMR}=\frac{2P_{eff}P'_{eff}}{1+P_{eff}P'_{eff}} \tag{3}$$

with the effective spin polarizations P_{eff} and P'_{eff} for the two electrodes,

$$P_{eff}=\frac{(k_\uparrow-k_\downarrow)}{(k_\uparrow+k_\downarrow)}\frac{(\kappa^2-k_\uparrow k_\downarrow)}{(\kappa^2+k_\uparrow k_\downarrow)}=P\frac{(\kappa^2-k_\uparrow k_\downarrow)}{(\kappa^2+k_\uparrow k_\downarrow)}, \tag{4}$$

$$P'_{eff}=\frac{(k'_\uparrow-k'_\downarrow)}{(k'_\uparrow+k'_\downarrow)}\frac{(\kappa^2-k'_\uparrow k'_\downarrow)}{(\kappa^2+k'_\uparrow k'_\downarrow)}=P'\frac{(\kappa^2-k'_\uparrow k'_\downarrow)}{(\kappa^2+k'_\uparrow k'_\downarrow)}, \tag{5}$$

where $k_\uparrow, k_\downarrow$ are the Fermi wave numbers in the up-spin and down-spin bands and κ is the wave number in the barrier. The two former factors at the right-hand sides of Eqs. (4) and (5) are the usual spin polarizations of the FM electrodes, which arise from the effects of the DOS as shown in Eq. (2). The two latter factors originate from the quantum-mechanical matching of the electron wave functions at the two electrode/barrier interfaces. They reflect the quantum coherence among the barrier and the two electrodes. However, they are totally absent in Eq. (1) of the Jullière model.

Recently, many experiments have been performed to measure the bias dependence of TMR for various ferromagnetic junctions within a wide range of applied voltage (about from -1.0 V to 1.0 V). Most of the results show a significant decrease of TMR with increasing voltage.[9] Interestingly, Sharma *et al.*[10] found that the TMR of junctions with pure Ta_2O_5 barrier undergoes a negative excursion at high enough positive and negative voltages, i.e., the TMR changes its sign at a large and finite voltage. In contrast, the junctions with the same electrodes, but with different barriers (e.g., Al_2O_3), exhibit mostly positive TMR in a decaying way before the damage (breakdown) voltage of the junctions. (Experimentally, beyond this voltage, the dielectric oxide barrier will be broken down due to the smallness of the barrier thickness

and its resulting strong electric field.) Different from those symmetrical barrier junctions, the composite barrier (e.g., Al_2O_3/Ta_2O_5) junctions are found to undergo a negative excursion of TMR at one side of the applied voltage, but remain unchanged in sign at the other side. If the composite barrier is reversed, for example, Al_2O_3/Ta_2O_5 is substituted by Ta_2O_5/Al_2O_3, the negative excursion is reversed from one side to the other side of the applied voltage. Regrettably, the expected inversion symmetry of the TMR versus voltage upon reversion is not observed in Ref. 10. Obviously, to interpret those behaviors of TMR, one needs a microscopic tunneling theory suitable for large applied voltages. However, the Slonczewski model is confined only to the zero bias. The purpose of this paper is to extend the Slonczewski model to the finite bias case, and we hope that it could provide a reasonable explanation to the strong bias dependence of TMR within a wide range of applied voltage. To this end, we will treat the electrodes and the barrier as a single quantum-mechanical system to include the quantum coherence which is physically essential for such a sandwich structure. Specifically, we will employ the WKB wave functions to describe the potential barrier and then match the wave functions and their derivatives at the electrode/barrier interfaces quantum mechanically. Our results show that the TMR decreases significantly with the increase of the applied voltage. In particular, the TMR can change from positive to negative at a finite voltage due to the quantum coherence. Furthermore, the effects of an asymmetric potential of the composite barrier have also been given. These results are qualitatively in agreement with the experiments.

The rest of the paper is organized as follows. In Sec. II, we extend the Slonczewski model by matching quantum mechanically the wave function through trapezoidal barrier due to the finite applied voltage, and obtain the bias-dependent rather than bias-independent transmission probabilities. In Sec. III, numerical results and theoretical analyses for both symmetrical and asymmetrical barriers are given. Finally, our results are summarized in Sec. IV.

II. EXTENSION OF THE SLONCZEWSKI MODEL

Here we consider a junction consisting of two identical ferromagnetic electrodes and a nonmagnetic insulating barrier. As usual, we will treat the ferromagnetic metals with the free-electron approximation because it has been adopted widely and achieved great success in describing the spin-polarized tunneling.[7,8,11,12] Within this approximation, the DOS for the two spin bands of the ferromagnetic electrodes are parabolic, which are depicted in Fig. 1. With the parabolic DOS's, the model of the FM/I/FM sandwich system can be described as

$$H_L = -\frac{\hbar^2}{2m}\frac{d^2}{dx^2} - \sigma_L\Delta + \phi(x), \tag{6}$$

$$H_B = -\frac{\hbar^2}{2m}\frac{d^2}{dx^2} + \phi(x), \tag{7}$$

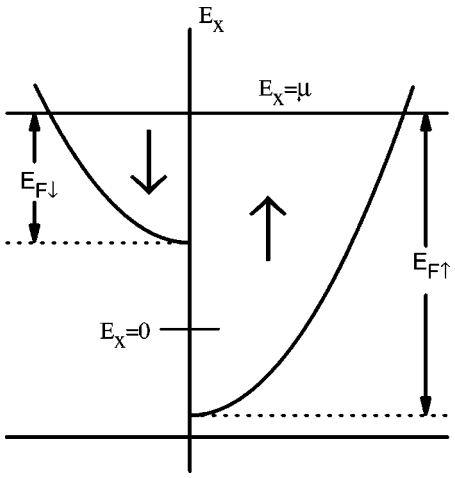

FIG. 1. The densities of states for the up-spin and down-spin bands, showing positions of the energy zero and chemical potential μ for the ferromagnetic electrode.

$$H_R = -\frac{\hbar^2}{2m}\frac{d^2}{dx^2} - \sigma_R\Delta + \phi(x), \tag{8}$$

where H_L, H_R, and H_B are the longitudinal parts of the Hamiltonians for the left and right electrodes and the barrier, respectively; Δ half the exchange splitting between the two spin bands of the ferromagnetic electrodes; σ_L and σ_R the conventional spin indices; and $\phi(x)$ the single-particle potential. We note that, in our model, the difference between the effective masses of the electrons within the barrier and the electrodes is neglected, just as in the Slonczewski model.[8] This simplification can reduce the adjustable parameters in the model and will not alter the theoretical conclusion qualitatively. The lateral (in-plane) parts of the Hamiltonians are assumed to be the simple free-electron type, and their effects will be accounted for by summing over the transverse momentum k_t in our later calculations. For convenience, the energy zero is selected at the center of the exchange splitting of the left electrode, so the potential $\phi(x)$ takes the following form:

$$\phi(x) = \begin{cases} 0, & x \leqslant 0 \\ \phi_L + \dfrac{x}{d}(\phi_R - \phi_L - eV), & 0 < x < d \\ -eV, & x \geqslant d, \end{cases} \tag{9}$$

where d is the barrier width; V the applied voltage; and ϕ_L and ϕ_R the barrier potentials at the left and right barrier/electrode interfaces. This potential is shown schematically in Fig. 2. It should be pointed out here that the barrier potential $\phi(x)$ $(0<x<d)$ is a function of the applied voltage V, different from the Slonczewski model[8] where $V=0$ and $\phi_L = \phi_R$, that is, only the zero-bias case is taken into account and the barrier potential is of square shape. Inclusion of V in the potential $\phi(x)$ enables us to easily investigate the TMR at large and finite applied voltage. Furthermore, just as Brinkman and co-workers,[3] we do not assume the barrier potential in Eq. (9) to be square even at zero bias. Often, this

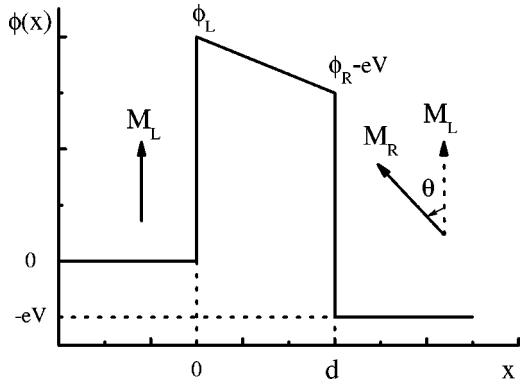

FIG. 2. A schematic potential for the FM/I/FM junction under the bias $V>0$ where the spin-quantization axes between the two ferromagnetic electrodes form angle θ.

would happen when unequal degree of oxidations occurs on each side of the insulator, or when the junction is fabricated with a composite barrier such as Al_2O_3/Ta_2O_5 insulator.[10]

First, we consider the case that a spin-up incident plane wave with longitudinal energy E_x and unit flux transports from the left electrode to the right electrode. For the electrode regions, $x\leqslant 0$ and $x\geqslant d$, the potential $\phi(x)$ is assumed to be constant, as indicated in Eq. (9). Therefore, the solutions to Hamiltonians H_L and H_R are simply plane waves,

$$\psi_{L\uparrow}(x)=k_{L\uparrow}^{-1/2}e^{ik_{L\uparrow}x}+R_{\uparrow}e^{-ik_{L\uparrow}x} \quad (x\leqslant 0),$$

$$\psi_{L\downarrow}(x)=R_{\downarrow}e^{-ik_{L\downarrow}x} \quad (x\leqslant 0),$$

$$\psi_{R\uparrow}(x)=C_{\uparrow}e^{ik_{R\uparrow}(x-d)} \quad (x\geqslant d),$$

$$\psi_{R\downarrow}(x)=C_{\downarrow}e^{ik_{R\downarrow}(x-d)} \quad (x\geqslant d), \tag{10}$$

where

$$k_{L\sigma_L}(E_x)=\left(\frac{2m}{\hbar^2}\right)^{1/2}\sqrt{E_x+\sigma_L\Delta}, \tag{11}$$

$$k_{R\sigma_R}(E_x,V)=\left(\frac{2m}{\hbar^2}\right)^{1/2}\sqrt{E_x+eV+\sigma_R\Delta}, \tag{12}$$

with $\sigma_L,\sigma_R=\pm 1$ corresponding to the spin orientation $\uparrow,\downarrow$, respectively. Here we have assumed that the up spin is the majority spin. Inside the barrier, $0<x<d$, the potential $\phi(x)$ becomes now trapezoidal instead of rectangular. With this linear potential, the Schrödinger equation for the Hamiltonian H_B of Eq. (7) can be solved rigorously by employing the Airy function. However, the use of the Airy function is too complex to get analytical results. Therefore, we turn to the WKB approximation.[13] This approximation has been successfully used to study the tunneling in the conventional junction with two paramagnetic electrodes in Refs. 2 and 3. As a result, the wave functions within the barrier region take the form,

$$\psi_{B\uparrow}(x)=[\kappa(E_x,x,V)]^{-1/2}\left[A_{\uparrow}\exp\left(-\int_0^x\kappa(E_x,x,V)dx\right)+B_{\uparrow}\exp\left(\int_0^x\kappa(E_x,x,V)dx\right)\right] \quad (0<x<d),$$

$$\psi_{B\downarrow}(x)=[\kappa(E_x,x,V)]^{-1/2}\left[A_{\downarrow}\exp\left(-\int_0^x\kappa(E_x,x,V)dx\right)+B_{\downarrow}\exp\left(\int_0^x\kappa(E_x,x,V)dx\right)\right] \quad (0<x<d), \tag{13}$$

where

$$\kappa(E_x,x,V)=\left(\frac{2m}{\hbar^2}\right)^{1/2}\sqrt{\phi_L+\frac{x}{d}(\phi_R-\phi_L-eV)-E_x}. \tag{14}$$

The WKB wave functions in Eq. (13) are applicable within the barrier region if the potential shape is smooth in the interval $0<x<d$. Just as pointed out by Harrison[2] and Brinkman,[3] even if the potential $\phi(x)$ varies abruptly at the interfaces $x=0$ and $x=d$, the wave functions (13) can still be connected with the wave functions (10) at $x=0$ and $x=d$ by a full quantum-mechanical matching. As will be seen later on, the above WKB wave functions are quite convenient for us to discuss the bias dependence of the TMR analytically. On the other hand, the wave functions of Eq. (13) reduce to the ones derived by Slonczewski[8] if $V=0$ and $\phi_L=\phi_R$. In Eqs. (10) and (13), $R_{\uparrow}$, $R_{\downarrow}$, $A_{\uparrow}$, $A_{\downarrow}$, $B_{\uparrow}$, $B_{\downarrow}$, $C_{\uparrow}$, and $C_{\downarrow}$ are coefficients, which will be determined by quantum-mechanical matching in the following.

Setting the angle of the spin-quantization axes for the two ferromagnetic electrodes to be θ, the boundary conditions for the quantum-mechanical matching among the wave functions [Eqs. (10) and (13)] and their derivatives can be written as

$$\psi_{L\uparrow}(0)=\psi_{B\uparrow}(0), \tag{15}$$

$$\psi_{L\downarrow}(0)=\psi_{B\downarrow}(0), \tag{16}$$

$$\psi'_{L\uparrow}(0)=\psi'_{B\uparrow}(0), \tag{17}$$

$$\psi'_{L\downarrow}(0)=\psi'_{B\downarrow}(0), \tag{18}$$

$$\psi_{B\uparrow}(d)=\psi_{R\uparrow}(d)\cos\left(\frac{\theta}{2}\right)+\psi_{R\downarrow}(d)\sin\left(\frac{\theta}{2}\right), \tag{19}$$

$$\psi_{B\downarrow}(d)=-\psi_{R\uparrow}(d)\sin\left(\frac{\theta}{2}\right)+\psi_{R\downarrow}(d)\cos\left(\frac{\theta}{2}\right), \tag{20}$$

$$\psi'_{B\uparrow}(d)=\psi'_{R\uparrow}(d)\cos\left(\frac{\theta}{2}\right)+\psi'_{R\downarrow}(d)\sin\left(\frac{\theta}{2}\right), \tag{21}$$

$$\psi'_{B\downarrow}(d)=-\psi'_{R\uparrow}(d)\sin\left(\frac{\theta}{2}\right)+\psi'_{R\downarrow}(d)\cos\left(\frac{\theta}{2}\right), \tag{22}$$

where a spinor transformation is performed in Eqs. (19)–(22) at the interface of $x=d$, because the spin-quantization axes for the two electrodes differ by an angle θ, as shown in Fig. 2.

If a spin-up electron tunnels from left electrode into right electrode and occupies the spin-up state of the right electrode, the corresponding transmission coefficient is

$$T_{\uparrow\uparrow}(E_x,V,\theta)=k_{R\uparrow}(E_x,V)|C_\uparrow|^2, \tag{23}$$

and if it occupies the spin-down state of the right electrode, the transmission coefficient becomes

$$T_{\uparrow\downarrow}(E_x,V,\theta)=k_{R\downarrow}(E_x,V)|C_\downarrow|^2. \tag{24}$$

The unknown coefficients $C_\uparrow$ and $C_\downarrow$ can be determined by Eqs. (10)–(22), following Harrison[2] and Brinkman.[3] The expressions for $T_{\uparrow\uparrow}$ and $T_{\uparrow\downarrow}$ are obtained as

$$T_{\uparrow\uparrow}(E_x,V,\theta)=\frac{16k_{L\uparrow}(E_x)k_{R\uparrow}(E_x,V)\kappa_L(E_x)\kappa_R(E_x,V)}{[\kappa_L^2(E_x)+k_{L\uparrow}^2(E_x)][\kappa_R^2(E_x,V)+k_{R\uparrow}^2(E_x,V)]}\times\cos^2\left(\frac{\theta}{2}\right)e^{-2\eta(E_x,V)}, \tag{25}$$

$$T_{\uparrow\downarrow}(E_x,V,\theta)=\frac{16k_{L\uparrow}(E_x)k_{R\downarrow}(E_x,V)\kappa_L(E_x)\kappa_R(E_x,V)}{[\kappa_L^2(E_x)+k_{L\uparrow}^2(E_x)][\kappa_R^2(E_x,V)+k_{R\downarrow}^2(E_x,V)]}\times\sin^2\left(\frac{\theta}{2}\right)e^{-2\eta(E_x,V)}, \tag{26}$$

where

$$\eta(E_x,V)=\int_0^d\kappa(E_x,x,V)dx, \tag{27}$$

and κ_L and κ_R are obtained from Eq. (14) as follows:

$$\kappa_L(E_x)=\kappa(E_x,0,V)=\left(\frac{2m}{\hbar^2}\right)^{1/2}\sqrt{\phi_L-E_x}, \tag{28}$$

$$\kappa_R(E_x,V)=\kappa(E_x,d,V)=\left(\frac{2m}{\hbar^2}\right)^{1/2}\sqrt{\phi_R-eV-E_x}. \tag{29}$$

Similarly, for the case that a spin-down incident plane wave with longitudinal energy E_x and unit flux transports from the left electrode to the right electrode, the two transmission coefficients are

$$T_{\downarrow\uparrow}(E_x,V,\theta)=\frac{16k_{L\downarrow}(E_x)k_{R\uparrow}(E_x,V)\kappa_L(E_x)\kappa_R(E_x,V)}{[\kappa_L^2(E_x)+k_{L\downarrow}^2(E_x)][\kappa_R^2(E_x,V)+k_{R\uparrow}^2(E_x,V)]}\times\sin^2\left(\frac{\theta}{2}\right)e^{-2\eta(E_x,V)}, \tag{30}$$

$$T_{\downarrow\downarrow}(E_x,V,\theta)=\frac{16k_{L\downarrow}(E_x)k_{R\downarrow}(E_x,V)\kappa_L(E_x)\kappa_R(E_x,V)}{[\kappa_L^2(E_x)+k_{L\downarrow}^2(E_x)][\kappa_R^2(E_x,V)+k_{R\downarrow}^2(E_x,V)]}\times\cos^2\left(\frac{\theta}{2}\right)e^{-2\eta(E_x,V)}. \tag{31}$$

With Eqs. (25), (26), (30), and (31), the tunneling current densities for parallel ($\theta=0$) and antiparallel ($\theta=\pi$) alignments, $J_P(V)$ and $J_{AP}(V)$, can be represented[1–3] as

$$J_P(V)=-\frac{e}{h}\sum_{k_t}\int_{-\infty}^{+\infty}dE_x\mathrm{P1}(E_x,V)\exp[-2\eta(E_x,V)]\times[f(E)-f(E-eV)], \tag{32}$$

$$J_{AP}(V)=-\frac{e}{h}\sum_{k_t}\int_{-\infty}^{+\infty}dE_x\mathrm{P2}(E_x,V)\exp[-2\eta(E_x,V)]\times[f(E)-f(E-eV)], \tag{33}$$

where the summation over k_t represents the contribution from the lateral part; E denotes the total energy of the tunneling electron; $f(E)$ the Fermi distribution function; $\exp[-2\eta(E_x,V)]$ the exponential weighting factor in the WKB approximation; P1 and P2 stand for the prefactors in Eqs. (32) and (33) which are given by

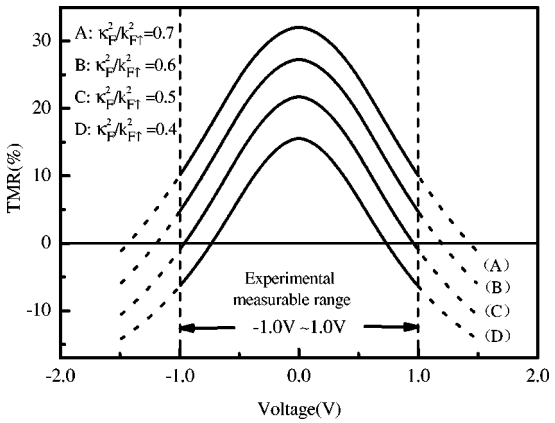

FIG. 3. The curves of the TMR vs bias for symmetric barrier junctions where $E_{F\uparrow}=5.0$ eV, $k_{F\downarrow}/k_{F\uparrow}=0.30$, and $d=15$ Å. The curves *A*, *B*, *C*, and *D* correspond to $\kappa_F^2/k_{F\uparrow}^2=0.7$, 0.6, 0.5, and 0.4, respectively.

$$\mathrm{P1}(E_x,V) \equiv \sum_{\sigma,\sigma'} T_{\sigma\sigma'}(E_x,V,0)\exp[2\eta(E_x,V)] = \frac{16k_{L\uparrow}(E_x)k_{R\uparrow}(E_x,V)\kappa_L(E_x)\kappa_R(E_x,V)}{[\kappa_L^2(E_x)+k_{L\uparrow}^2(E_x)][\kappa_R^2(E_x,V)+k_{R\uparrow}^2(E_x,V)]} + \frac{16k_{L\downarrow}(E_x)k_{R\downarrow}(E_x,V)\kappa_L(E_x)\kappa_R(E_x,V)}{[\kappa_L^2(E_x)+k_{L\downarrow}^2(E_x)][\kappa_R^2(E_x,V)+k_{R\downarrow}^2(E_x,V)]}, \tag{34}$$

$$\mathrm{P2}(E_x,V) \equiv \sum_{\sigma,\sigma'} T_{\sigma\sigma'}(E_x,V,\pi)\exp[2\eta(E_x,V)] = \frac{16k_{L\uparrow}(E_x)k_{R\downarrow}(E_x,V)\kappa_L(E_x)\kappa_R(E_x,V)}{[\kappa_L^2(E_x)+k_{L\uparrow}^2(E_x)][\kappa_R^2(E_x,V)+k_{R\downarrow}^2(E_x,V)]} + \frac{16k_{L\downarrow}(E_x)k_{R\uparrow}(E_x,V)\kappa_L(E_x)\kappa_R(E_x,V)}{[\kappa_L^2(E_x)+k_{L\downarrow}^2(E_x)][\kappa_R^2(E_x,V)+k_{R\uparrow}^2(E_x,V)]}. \tag{35}$$

If the electrodes are paramagnetic instead of ferromagnetic, Eqs. (32) and (33) automatically reduce to the result of Brinkman.[3] In other words, Brinkman's result[3] for nonmagnetic junctions has already been included in the present theory. In analogy to Ref. 3, the prefactors P1 and P2 in Eqs. (32) and (33) depend heavily on the energy E_x and the applied voltage V. They can impose a strong influence on the tunneling currents and will play a crucial role in the sign change of TMR, as can be seen in the following section.

Experimentally, the tunneling conductance and the TMR are defined as

$$G_P(V) = \frac{J_P(V)}{V}, \tag{36}$$

$$G_{AP}(V) = \frac{J_{AP}(V)}{V}, \tag{37}$$

$$\mathrm{TMR} \equiv \frac{G_P(V)-G_{AP}(V)}{G_P(V)} = \frac{\Delta G(V)}{G_P(V)}, \tag{38}$$

where $G_P(V)$ and $G_{AP}(V)$ are the tunneling conductance of the parallel and antiparallel alignments, respectively, and $\Delta G(V) \equiv G_P(V) - G_{AP}(V)$. Now, the TMR can be calculated through Eqs. (11), (12), (28), (29), and (32)–(38). Here, we emphasize that the above derivation is proceeded under the condition of a finite applied voltage. Therefore, the bias dependence of TMR can be obtained within a wide range of the applied voltage.

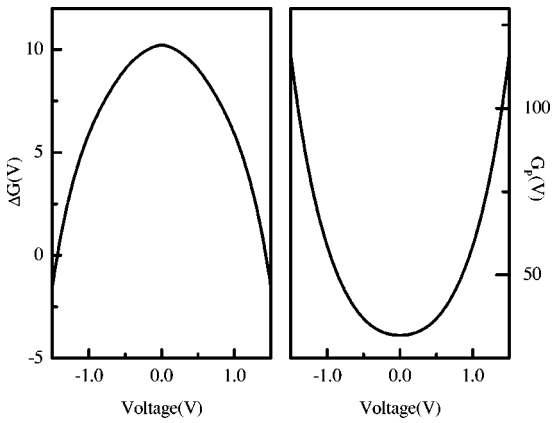

FIG. 4. The curves of ΔG and G_P vs V where $E_{F\uparrow}=5.0$ eV, $k_{F\downarrow}/k_{F\uparrow}=0.30$, $\kappa_F^2/k_{F\uparrow}^2=0.7$, and $d=15$ Å.

III. NUMERICAL RESULTS AND DISCUSSION

Following Slonczewski,[8] four parameters are needed for numerical evaluations: $E_{F\uparrow}$, $\kappa_F^2/k_{F\uparrow}^2$, $k_{F\downarrow}/k_{F\uparrow}$, and d, where $E_{F\uparrow}$ represents the Fermi energy of the spin-up electrons in the ferromagnetic electrodes; $\kappa_F^2/k_{F\uparrow}^2=(2m/\hbar^2)(\overline{\phi}-\mu)/E_{F\uparrow}$ the relative barrier height with μ the chemical potential and $\overline{\phi}=1/2(\phi_L+\phi_R)$; $k_{F\downarrow}/k_{F\uparrow}$ the ratio of the Fermi wave numbers for different spin bands; and d the barrier width.

First, we consider the junctions with a symmetric barrier ($\phi_L=\phi_R$), the numerical results at zero temperature calculated through Eqs. (11), (12), (28), (29), and (32)–(38) are shown in Fig. 3 where the curves *A*, *B*, *C*, and *D* correspond to $\kappa_F^2/k_{F\uparrow}^2=0.7$, 0.6, 0.5, and 0.4, respectively. As can be seen clearly, the TMR's decrease quickly with the increase of the applied voltage V, and finally change from positive to negative at a critical bias V_c. Moreover, the higher the barrier potential, the larger the critical voltage V_c will be. However, within the experimental measurable range of the applied voltage (from -1.0 V to 1.0 V), one sees that the TMR changes sign for the junctions with low barrier potentials (curves *C* and *D*), but still remains positive for junctions with high barrier potentials (curves *A* and *B*). The curves *A* and *B* can be used to explain experimental data of the TMR for junctions with Al_2O_3 barrier where no inverse TMR is observed before the damage (breakdown) voltage; the curves *C* and *D* can be used to explain the appearance of inverse TMR in junctions with Ta_2O_5 barrier.[10]

To understand the rapid decreasing of TMR, we have calculated $\Delta G(V)$ and $G_P(V)$, which are shown in Fig. 4. As indicated by Fig. 4, $\Delta G(V)$ decreases with the applied voltage V. In particular, $G_P(V)$ increases rapidly with V, which, as is well known, is due to the WKB exponential weighting factor. Consequently, the TMR defined in Eq. (38) must drop significantly with increasing V.

We now discuss the origin of the sign change in TMR. From Eqs. (36)–(38), we have

$$\mathrm{TMR} = \frac{J_P(V)-J_{AP}(V)}{J_P(V)} = \frac{\Delta J(V)}{J_P(V)}, \tag{39}$$

where $\Delta J(V)=J_P(V)-J_{AP}(V)$. Substituting $J_P(V)$ of Eq. (32) and $J_{AP}(V)$ of Eq. (33) into $\Delta J(V)$, we find

$$\Delta J(V)=-\frac{e}{h}\sum_{k_t}\int_{-\infty}^{+\infty}dE_x[\mathrm{P1}(E_x,V)-\mathrm{P2}(E_x,V)]\times\exp[-2\eta(E_x,V)][f(E)-f(E-eV)]. \quad (40)$$

As for $\mathrm{P1}(E_x,V)-\mathrm{P2}(E_x,V)$, by using Eqs. (34) and (35), it can be separated into two factors,

$$\mathrm{P1}(E_x,V)-\mathrm{P2}(E_x,V)=A(E_x,V)D(E_x,V), \quad (41)$$

where

$$A(E_x,V)=\frac{4\kappa_L(E_x)[k_{L\uparrow}(E_x)-k_{L\downarrow}(E_x)][\kappa_L^2(E_x)-k_{L\uparrow}(E_x)k_{L\downarrow}(E_x)]}{[\kappa_L^2(E_x)+k_{L\uparrow}^2(E_x)][\kappa_L^2(E_x)+k_{L\downarrow}^2(E_x)]}\frac{4\kappa_R(E_x,V)[k_{R\uparrow}(E_x,V)-k_{R\downarrow}(E_x,V)]}{[\kappa_R^2(E_x,V)+k_{R\uparrow}^2(E_x,V)][\kappa_R^2(E_x,V)+k_{R\downarrow}^2(E_x,V)]}, \quad (42)$$

$$D(E_x,V)=\kappa_R^2(E_x,V)-k_{R\uparrow}(E_x,V)k_{R\downarrow}(E_x,V). \quad (43)$$

The factors $A(E_x,V)$ and $D(E_x,V)$ show different behaviors with increasing voltage, which we will discuss in the following.

From Eqs. (11), (12), and (14), we have

$$k_{L\uparrow}(E_x)-k_{L\downarrow}(E_x)=\left(\frac{2m}{\hbar^2}\right)^{1/2}[\sqrt{E_x+\Delta}-\sqrt{E_x-\Delta}]>0, \quad (44)$$

$$k_{R\uparrow}(E_x,V)-k_{R\downarrow}(E_x,V)=\left(\frac{2m}{\hbar^2}\right)^{1/2}[\sqrt{E_x+eV+\Delta}-\sqrt{E_x+eV-\Delta}]>0, \quad (45)$$

$$[\kappa_L^2(E_x)-k_{L\uparrow}(E_x)k_{L\downarrow}(E_x)]>0. \quad (46)$$

Equations (44) and (45) are satisfied simply because the spin-up band has been assumed to be the majority band, and Eq. (46) is satisfied because the effective polarization of the left ferromagnetic electrode, P_{eff} of Eq. (4), is chosen to be positive, as is the usual case for experimental ferromagnetic metals. Their combination results in

$$A(E_x,V)>0.$$

Obviously, the factor $A(E_x,V)$ is always positive and does not change in sign regardless of the magnitude of the applied voltage. As stated above, this result is due to the DOS effect of the FM electrodes.

As to the other factor $D(E_x,V)$, one finds

$$D(E_x,V)=\left(\frac{2m}{\hbar^2}\right)[(\phi_R-E_x-eV)-\sqrt{(E_x+eV)^2-\Delta^2}]. \quad (47)$$

The first term on the right-hand side comes from the contribution of $\kappa_R^2(E_x,V)$ given in Eq. (29), and the second one from the contribution of $k_{R\uparrow}(E_x,V)k_{R\downarrow}(E_x,V)$ given in Eq. (12). The former, i.e., $\kappa_R^2(E_x,V)$, decreases with the increase of V, but the latter, i.e., $k_{R\uparrow}(E_x,V)k_{R\downarrow}(E_x,V)$, increases with V. Therefore, $D(E_x,V)$ is a rapidly decreasing function of V, and it will change from positive to negative if the applied voltage V is sufficiently high. Clearly, this property of $D(E_x,V)$ is not the DOS effect of the FM electrodes, different from that of $A(E_x,V)$. As a combined result of $A(E_x,V)$ and $D(E_x,V)$, $\mathrm{P1}(E_x,V)-\mathrm{P2}(E_x,V)$ of Eq. (41) will become negative at certain bias. Apparently, the sign change originates from the quantum-coherence factor $D(E_x,V)$ in our model rather than the DOS effect included in $A(E_x,V)$. On the other hand, the terms other than $\mathrm{P1}(E_x,V)-\mathrm{P2}(E_x,V)$ in the integrand of Eq. (40) do not change sign for any V. Therefore, $\Delta J(V)$ of Eq. (40) and the TMR of Eq. (39) will finally undergo a sign change at a sufficiently large critical voltage V_c.

The above discussions show that the microscopic mechanism responsible for the sign change of TMR is due to the quantum coherence effect rather than the DOS effect. There exist two terms in the quantum-coherence factor $D(E_x,V)$, i.e., $\kappa_R^2(E_x,V)$ and $k_{R\uparrow}(E_x,V)k_{R\downarrow}(E_x,V)$. Physically, $\kappa_R^2(E_x,V)$ can be considered, on an average, as the potential barrier height. The higher (lower) the potential barrier, the larger (smaller) the tunneling magnetoresistance. On the other hand, $k_{R\uparrow}(E_x,V)$ and $k_{R\downarrow}(E_x,V)$ are directly proportional to the transmission coefficient, as shown in Eqs. (23) and (24). The larger the transmission coefficient, the lower the tunneling magnetoresistance. If the applied voltage increases, then the average height of the potential barrier decreases, and the transmission coefficient increases. Therefore, with the increase of the applied voltage, the tunneling magnetoresistance will decrease rapidly and finally change its sign. This is the microscopic reason for the sign change of TMR in the present model.

Now, we proceed to estimate the critical voltage V_c where the TMR changes sign. Because electrons with energy E_x near the Fermi level (i.e., the chemical potential μ at zero temperature) give most contributions to the tunneling current, we can obtain the estimated critical voltage V_{est} by approximating $D(\mu,V_{est})=0$, which results in

$$eV_{est}=\frac{1}{2}\phi_R+\frac{\Delta^2}{2\phi_R}-\mu. \quad (48)$$

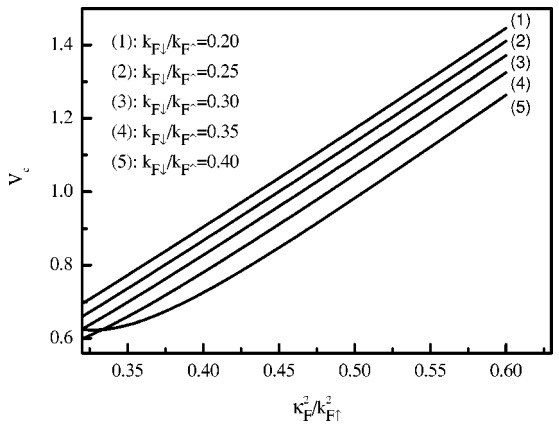

FIG. 5. The curves of V_c vs $\kappa_F^2/k_{F\uparrow}$ where $E_{F\uparrow}=5.0$ eV and $d=15$ Å. The curves (1), (2), (3), (4), and (5) correspond to $k_{F\downarrow}/k_{F\uparrow}=0.20$, 0.25, 0.30, 0.35, and 0.40, respectively.

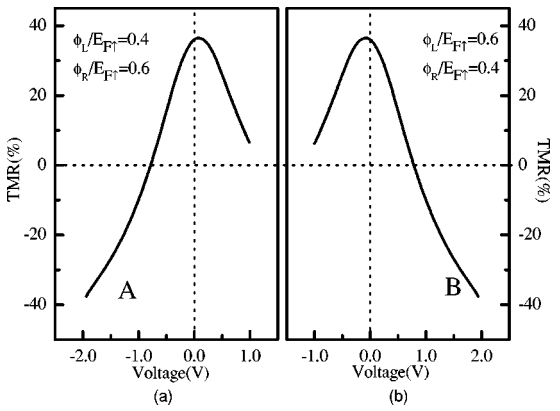

FIG. 6. The curves of the TMR versus bias for asymmetric barrier junctions where $E_{F\uparrow}=5.0$ eV, $k_{F\downarrow}/k_{F\uparrow}=0.30$, and $d=15$ Å. The curve (a) is for the case of $\phi_L/E_{F\uparrow}=0.4$ and $\phi_R/E_{F\uparrow}=0.6$ and the curve (b) for the case of $\phi_L/E_{F\uparrow}=0.6$ and $\phi_R/E_{F\uparrow}=0.4$.

Equation (48) shows that V_{est} depends linearly on ϕ_R for a sufficiently high barrier potential ϕ_R. In fact, we have calculated the exact numerical value of V_c as a function of $\kappa_F^2/k_{F\uparrow}^2$ for different values of $k_{F\downarrow}/k_{F\uparrow}$ from Eqs. (32)–(38), the results are shown in Fig. 5. All the curves in Fig. 5 show a good linear dependence between V_c and $\kappa_F^2/k_{F\uparrow}^2$ for relatively large $\kappa_F^2/k_{F\uparrow}^2$, and also, a higher relative barrier height $\kappa_F^2/k_{F\uparrow}^2$ leads to a higher critical voltage V_c, which is in agreement with the qualitative analysis of Eq. (48). This relationship between V_c and the relative barrier height can be used to explain why no sign change is observed in ferromagnetic junctions with Al_2O_3 barrier. For Al_2O_3 barrier, the relative barrier height is rather large, its critical voltage V_c is so high that the junction will undergo permanent damage before the TMR changes sign.

Second, we consider the junctions with asymmetric barrier ($\phi_L \neq \phi_R$). To simplify the calculation, the influence of the tunneling electron effective mass and the barrier shape due to different barrier heights on the two side of the barrier will not be included. Two cases are considered in our calculation: $\phi_L/E_{F\uparrow}=0.4$ and $\phi_L/E_{F\uparrow}=0.6$, and their reversal, i.e., $\phi_L/E_{F\uparrow}=0.6$ and $\phi_L/E_{F\uparrow}=0.4$. The numerical results are shown in Figs. 6(a) and 6(b), respectively. It is clear that the inverse TMR only occurs at one side of the applied voltage, in contrast to the case with symmetric barrier shown in Fig. 3 where inverse TMR appears at both sides. The asymmetry of TMR due to $\phi_L \neq \phi_R$ is in accordance with the experimental results of composite barrier (Al_2O_3/Ta_2O_5 and Ta_2O_5/Al_2O_3) junctions reported by Sharma and co-workers.[10] Although the expected mirror symmetry between Figs. 6(a) and 6(b) is not observed in their experiments, we believe that this inversion should be observed experimentally. Recently, we have been informed[14] that TMR curves of Al_2O_3/ZrO_2 junction and ZrO_2/Al_2O_3 actually exhibit a good inversion symmetry as expected. Incidentally, as indicated in Figs. 6(a) and 6(b), the maximum of the TMR deviates from the position of $V=0$, namely, there is an offset in the TMR when the barrier potential is asymmetric. This behavior has also been observed experimentally.[15,16]

IV. CONCLUSIONS

By extending the Slonczewski model from a rectangular barrier potential to a trapezoidal barrier potential, we have presented a spin-polarized tunneling theory for the FM/I/FM junctions within a wide range of the applied voltage and provided a possible explanation to the sign change of the TMR. The trapezoidal potential within the barrier region is handled by the WKB approximation, and the wave functions are quantum-mechanically matched on the interfaces following the treatment by Harrison.[2] We found that, apart from the usual DOS effects, there exists a quantum-coherence factor $D(E_x,V)=\kappa_R^2(E_x,V)-k_{R\uparrow}(E_x,V)k_{R\downarrow}(E_x,V)$, which is of great importance for understanding the strong bias dependence of the tunneling, especially, the sign change in TMR with bias. Our theoretical results, including both symmetric and asymmetric barrier potentials, are in qualitative agreement with the experimental observations. The further application of the theory to the finite-temperature case is being worked on and will be published elsewhere.

ACKNOWLEDGMENTS

This work was supported by the State Key Project of Fundamental Research under Grant No. 001CB610602 and the National Science Foundation of China. The authors would like to thank Dr. John Q. Xiao for useful discussions and his critical reading of the manuscript.

[1] C. B. Duke, *Tunneling in Solids* (Academic, New York, 1969).
[2] W.A. Harrison, Phys. Rev. **123**, 85 (1961).
[3] W.F. Brinkman, R.C. Dynes, and J.M. Rowell, J. Appl. Phys. **41**, 1915 (1970).
[4] J.G. Simmons, J. Appl. Phys. **34**, 1793 (1963).
[5] P.M. Tedrow and R. Meservey, Phys. Rev. Lett. **26**, 192 (1971).
[6] M. Jullière, Phys. Lett. **54A**, 225 (1975).
[7] J.M. MacLaren, X.-G. Zhang, and W.H. Butler, Phys. Rev. B **56**, 11 827 (1997).
[8] J.C. Slonczewski, Phys. Rev. B **39**, 6995 (1989).
[9] J.S. Moodera and G. Mathon, J. Magn. Magn. Mater. **200**, 248 (1999).
[10] M. Sharma, S.X. Wang, and J.H. Nickel, Phys. Rev. Lett. **82**, 616 (1999).
[11] M.B. Stearns, J. Magn. Magn. Mater. **5**, 167 (1977).
[12] Xiangdong Zhang, Bo-Zhang Li, Gang Sun, and Fu-Cho Pu, Phys. Rev. B **56**, 5484 (1997).
[13] E. Merzbacher, *Quantum Mechanics*, 2nd ed. (Wiley, New York, 1970).
[14] John Q. Xiao (private communication).
[15] J. Nowak, D. Song, and E. Murdock, J. Appl. Phys. **87**, 5203 (2000).
[16] J. Du, X.H. Xiang, G. Landry, B. You, A. Hu, H.W. Zhao, and John Q. Xiao, J. Appl. Phys. **91**, 8780 (2002).